Title: A comparative physicochemical, morphological and magnetic study of silane-functionalized superparamagnetic iron oxide nanoparticles prepared by alkaline coprecipitation

Author: Laura-Karina Mireles Edward Sacher L'Hocine Yahia Sophie Laurent Dimitri Stanicki

PII: S1357-2725(15)30075-3
DOI: http://dx.doi.org/doi:10.1016/j.biocel.2015.12.002
Reference: BC 4753

To appear in: *The International Journal of Biochemistry & Cell Biology*

Received date: 27-8-2015
Revised date: 30-11-2015
Accepted date: 2-12-2015

Please cite this article as: Mireles, L.-K., Sacher, E., Yahia, L. H., Laurent, S., and Stanicki, D.,A comparative physicochemical, morphological and magnetic study of silane-functionalized superparamagnetic iron oxide nanoparticles prepared by alkaline coprecipitation, *International Journal of Biochemistry and Cell Biology* (2015), http://dx.doi.org/10.1016/j.biocel.2015.12.002

A comparative physicochemical, morphological and magnetic study of silane-functionalized superparamagnetic iron oxide nanoparticles prepared by alkaline coprecipitation.

Laura-Karina Mireles, [a*] Edward Sacher, [a,b] L'Hocine Yahia, [a] Sophie Laurent, [c,d] and Dimitri Stanicki [d]

[a] Laboratoire d'Innovation et d'Analyse de Bioperformance, École Polytechnique de Montréal, C.P. 6079, Succursale Centre-ville, Montréal, Québec H3C 3A7, Canada.
[b] Département de Génie physique, École Polytechnique de Montréal, C.P. 6079, Succursale Centre-ville, Montréal, Québec H3C 3A7, Canada.
[c] Department of General, Organic, Biomedical Chemistry, NMR and Molecular Imaging Laboratory, Université de Mons, 19 Avenue Maistriau, B-7000 Mons, Belgium.
[d] Center for Microscopy and Molecular Imaging (CMMI), B-6041 Gosselies, Belgium.

Contact e-mail: karina.mireles@polymtl.ca Telephone: (514) 340-4711, ext. 2838

Abstract

The characterization of synthetic superparamagnetic iron oxide nanoparticle (SPION) surfaces prior to functionalization is an essential step in the prediction of their successful functionalization, and in uncovering issues that may influence their selection as magnetically targeted drug delivery vehicles (prodrugs). Here, three differently functionalized magnetite (Fe_3O_4) SPIONs are considered. All were identically prepared by the alkaline coprecipitation of Fe^{2+} and Fe^{3+} salts. We use X-ray photoelectron spectroscopy, electron microscopy, time-of-flight SIMS, FTIR spectroscopy and magnetic measurements to characterize their chemical, morphological and magnetic properties, in order to aid in determining how their surfaces differ from those prepared by $Fe(CO)_5$ decomposition, which we have already studied, and in assessing their potential use as drug delivery carriers.

Key words*:* Drug delivery; magnetite; superparamagnetic nanoparticles; surface analysis; surface reproducibility; washing effect.

1. Introduction

Advances in the technology of nanoparticles used in drug delivery applications herald a promising future for their use in medicine. Currently many research teams are investigating targeted drug delivery for the treatment of cancers, (Davydov et al. 2014) and pulmonary, (Pham et al. 2015) cardiovascular (Rao et al 2014) and infectious diseases, (Davydov et al. 2014, Pham et al. 2015, Rao et al 2014, (Mbeh et al. 2012) among others. Our group, for example, is interested in nanocarriers that act against bacteria and are capable of preventing biofilm formation on implant surfaces, because nosocomial infections represent a huge health problem around the world: just in Canada, a quarter of a million cases of associated infections are reported annually. This fact results in 8,500-12,000 deaths, and the rate is rising. (Healthcare-associated Infections, 2009) Infections caused by *Staphylococcus epidermidis* and *Staphylococcus aureus* are the most common, and are present in 70-90% of reported cases of implant-related infections. (Dickinson et al. 1989) Our approach to the prevention of the bacterial adhesion is to develop functional coatings that are capable of destroying adhering bacteria. (Nablo et al. 2005) Antibiotics, (Trampuz et al 2001, Wilcox et al. 2001) silver ions (Yamanaka et al. 2005) and nitric oxide (NO), (Nablo et al. 2005) among others, have all shown antibacterial properties, reducing the amount of bacterial adhesion. Various vehicles have been proposed for use as prodrugs; these include nanoparticles, (França et al. 2013, Zhang et al. 2012) micelles (Zhang et al. 2012) and polymers. (França et al. 2013, Zhang et al. 2012)

We propose to use functionalized SPIONs to target the infected site. SPIONs are considered to be excellent candidates for drug delivery, (França et al. 2013) since they can be directed *in vivo* to the specific target sites using external magnetic fields, when their diameters are smaller than 100 nm. (Frankel et al 1997, Felfoul et al. 2010, Brosseau et al. 2003)

On attaining the target, they function as advanced medical tools. As examples, they may be used as prodrugs, (França et al. 2013, Zhang et al. 2012, Felfoul et al. 2010, Afkhami et al 2011) as contrast agents, (Felfoul et al. 2010, Afkhami et al 2011) in hyperthermia (Felfoul et al. 2010, Afkhami et al 2011, Liu et al. 2012) and in cancer treatment. (Afkhami et al 2011, Liu et al. 2012, Sawant et al. 2009) They possess low cytotoxicity and high biocompatibility, (Mbeh et al. 2012) and have been accepted by the United States Food and Drug Administration (FDA), both as prodrugs and for clinical MRI applications. (Gupta et al. 2004, Tassa et al. 2011) *In vivo,* SPIONs are converted to ferric ions, which are assimilated into the biological

iron storage pool, as erythrocytes, indicating their acceptable use in humans. (Li et al. 2011)

In a previous paper, we considered SPIONs manufactured by the thermal decomposition of $Fe(CO)_5$, whose mechanism is obscure: the nominally zero-valent Fe must oxidize to Fe^{2+} and Fe^{3+}, in the correct 1:2 ratio, before obtaining O, and forming Fe_3O_4 SPIONs. Their surfaces were found to be heavily contaminated during fabrication, (França et al. 2013) and they were found to have batch-to-batch variations of the surface chemistry, extensive enough to remove them from consideration as prodrugs. In fact, the general reproducibility of nanoparticle surface chemistry may presently be unfeasible. This presents a serious challenge for new biomedical applications, with their safety-related issues (protein corona formation, and the resultant bio- and hemocompatibilties) that depend on the control of the chemical and physical properties of the surfaces.

In the present paper, we characterize SPIONs made in a more conventional manner: the alkaline coprecipitation of Fe^{2+} and Fe^{3+}, in the correct 1:2 ratio; the precipitate loses water and forms Fe_3O_4 on annealing. SPIONs fabricated in this manner have been the subjects of several recent papers (Forge et al. 2008, Bridot et al. 2013). It is our purpose to thoroughly characterize them, to determine to what extent their surfaces differ from those made by the thermal decomposition of $Fe(CO)_5$, which we previously studied, (França et al. 2013) to what extent their synthesis is reproducible, and, through this, if they can be considered as potential candidates for use as prodrugs to target the infected sites.

2. Materials and methods

2.1 Synthesis

2.1.1 Bare SPIONs

Bare SPIONs were synthesized by the alkaline coprecipitation of iron salts in diethylene glycol (DEG), according to a published protocol. (Forge et al. 2008, Bridot et al. 2013) Briefly, a mixture of $FeCl_2.4H_2O$ (45 mmol; 8.9 g) and $FeCl_3$ (45% solution; 37 mmol; 9.1 ml) in DEG (250 ml) was heated under N_2 at 170°C, with stirring. After 15 min, solid NaOH (15 g) was added. After stirring for 1 h at 170°C, the solution was cooled and the magnetic particles were isolated by magnetic decantation (B_0 = 0. 5 T). The black precipitate was washed five times with aqueous HNO_3 (200 ml, 1 M) and the SPIONs were dispersed in deionized water, sonicated (45 min), and centrifuged (16, 500 G; 45 min) to remove aggregates (eq. 1).

$$2Fe^{3+} + Fe^{2+} + 8OH^{-} \longrightarrow Fe_3O_4 + 4H_2O$$

2.1.2 Positive SPIONs

TPED [N-[3-(trimethoxysilyl)propyl] ethylenediamine] (50 mmol; 10.8 ml) was slowly added to an aqueous suspension of bare SPIONs (200 ml; [Fe] = 25 mM) at 50°C and the mixture was heated at reflux for 2 h. On cooling, the suspension was purified by membrane filtration (membrane cut-off: 30 kDa), and centrifuged (16, 500 g; 45 min).

2.1.3 Negative SPIONs

Bare SPIONs were treated with TEPSA [3-(triethoxysilyl) propyl succinic anhydride] in organic medium, as previously described. (Bridot et al. 2013, Stanicki et al. 2014) Briefly, TEPSA (25 mmol; 7.1 ml) was slowly added to a suspension of SPIONs in dimethylformamide (50 ml; [Fe] = 100 mM). Water was then added (4.3 ml), followed by an aqueous solution of $(CH_3)_4NOH$ (1 M; 2.5 mmol; 2.5 ml) at room temperature while stirring. After heating at 100°C for 24 h under continuous stirring, the SPIONs were collected by pouring the suspension into an acetone/diethyl ether mixture, followed by magnetic decantation. After washing with acetone, the black precipitate was dispersed in water and purified by membrane filtration (membrane cut-off: 30 kDa) before centrifuging (16, 500 g; 45 min).

2.2 Characterizations

2.2.1 Transmission electron microscopy (TEM)

Photomicrographs were obtained by bright-field imaging, using a JEM-2100F electron microscope, at beam energy of 200 keV. The elemental analysis was carried out by energy dispersive spectroscopy (EDS). Selected area electronic diffraction (SAED) was used to obtain crystal diffraction patterns. All the samples were diluted in water before preparation, and sonicated for 3 minutes to disperse the SPIONs. One drop of each sample was spread onto a copper grid and covered with a microscope cover glass until dry.

2.2.2 Vibrating sample magnetometry

Vibrating sample magnetometry was used to obtain the magnetization vs. magnetic field (M vs H) loop at room temperature, from H= 0 - 2 T, with a measurement precision of $1x10^{-6}$ emu. Measurements were determined on a known quantity of sample. Drops of each sample were spread onto a 10 mm x 10 mm piece of cleaned glass, and dried, and the weight of each sample was obtained before the measurement.

2.2.3 Transmission IR spectroscopy

Transmission IR spectra were obtained, in the range 400 - 4000 cm^{-1}, using a Thermo Scientific Nicolet 6700 Fourier transform IR spectrometer, at a resolution of 4 cm^{-1}; 96 co-additions were used to increase S/N. The samples were deposited by placing a drop on a diamond plate, and drying before adding the next drop; spectra were obtained after depositing three drops.

2.2.4 X-ray photoelectron spectroscopy

X-ray photoelectron spectroscopy (XPS) was performed with a VG ESCALAB 3 MK II (Thermo VG Scientific), using non-monochromated Al Kα X-rays (hν = 1486.6 eV) at an instrument resolution of 0.85 eV and a perpendicular take-off angle. The analysis chamber pressure was < 10^{-9} torr. Following Shirley background removal, the component peaks were separated by the VG Avantage software. The energy was calibrated by setting the C1s C-C peaks of all but the negative SPIONs to 285 eV; the energy of the negative SPIONs was calibrated by setting the more prominent C-Si peak to 284.1 eV. FWHM values were those previously established in our laboratory. Drops were deposited onto highly oriented pyrolytic graphite (HOPG) and permitted to dry.

2.2.5 Time-of-flight SIMS

ToF-SIMS was carried out on an ION-TOF TOF-SIMS IV mass spectrometer, with a mono-isotopic Bi^+ beam, generated by a liquid metal gun mounted on the instrument. The beam current was 1.5 pA. Drops of the samples were deposited onto a silicon substrate, covering an area greater than 2 mm x 2 mm, and permitted to dry. Positive ion spectra were calibrated using H^+, H_2^+, and $C_xH_y^+$ peaks, and negative ion spectra used C^-, CH^-, C_2^-, C_2H^-, C_3^- and C_3H^- peaks.

3. Results

3.1 TEM *(Size distribution and morphology)*

TEM photomicrographs are found in Fig. 1, all SPIONs (Fig. 1a-c) had well-defined shapes; their selected area electron diffraction patterns correspond to Fe_3O_4.The size distributions can be observed in the histograms (Fig. 2), where the average diameters of bare, positive and negative SPIONs (Fig. 2a-c) are 9.2 ± 1.3, 9.7 ± 1.8 and 9.9 ± 1.1 nm, respectively.

3.2 VSM

Fig 3 contains the magnetization curves of the samples at room temperature. The absence of hysteresis loops confirms that the three SPIONs have superparamagnetic behavior. The saturation magnetization (M_s) values were 27 emu/g for the bare SPIONs, 28 emu/g for the positive SPIONs and 24 emu/g for the negative SPIONs, all at ~ 10 000 Oe.

3.3 XPS

In this section, the results of two batches of SPIONs are presented. A second batch was characterized because (1) the analysis of the first batch showed the presence of surface contaminants and (2) we wished to determine whether there were batch-to-batch inconsistencies.

SPION survey spectra, seen in the upper row of Fig. 4 (first batch) and Fig. 5 (second batch), revealed the presence of carbon, oxygen, iron, nitrogen and silicon. For pure Fe_3O_4, the chemical distribution of Fe ions would correspond to 1:1:1 Fe^{II} octahedral: Fe^{III}

octahedral: Fe^{III} tetrahedral. (Poulin et al.2010) In the spectra of all the SPIONs in Figs. 4 and 5, it is clear that none of the Fe^{II} octahedral (~ 709.6 eV): Fe^{III} octahedral (~ 710.2-711.7 eV): Fe^{III} tetrahedral (~ 712.9-713.7 eV) peaks of the SPIONs correspond to this ratio, probably due to incomplete surface oxidation, as well as chemical modifications that occurred during manufacture and functionalization.

3.3.1 Bare SPIONs

The spectra of the bare SPIONs, in Figs. 4 and 5, contain several contaminant peaks, such as oxidized C and NO_3^-, present even before functionalization. While peak attributions are found in Table 1, some peaks could not be attributed with certainty, due to contaminant interference, SPION catalysis and peak overlap.

3.3.2 Positive SPIONs

The pK_as of amines lie near 9, so that, in water (pH = 7), they are protonated ($-NH_3^+$) and, thus, positively charged. The deposition of aminosilanes, such as the TPED used here, is self-catalyzed (Kaas et al.1971) and, on deposition onto *flat plates*, results in surface layers several nm thick. However, HRTEM photomicrographs of all the SPIONs (Fig. 6) show the absence of such a layer, as does the absence of C1s peak components attributable to C-Si and C-N. Despite this, the presence of N1s and Si2p spectra indicates that at least *some* aminosilane molecules were deposited, probably as a monolayer or less. This lack of an expected silane layer is surely due to the fact that the Fe_3O_4 SPION is itself, a catalyst (Agnihotri et al. 2013) of certain reactions and, as the XPS component peaks in Table 1 indicate, is capable of causing unexpected reactions, such as the C and N oxidations and Si fragmentation, previously reported by us. (França et al. 2013, Zhang et al. 2012)

3.3.3 Negative SPIONs

The pK_as of carboxylic acids, obtained when the anhydride of the presently used TEPSA is hydrolyzed, lie near 4, so that, in water, they are ionized ($-COO^-$), and, thus, negatively charged. As noted earlier, HRTEM photomicrographs indicate the absence of a noticeable surface layer (Fig. 6), although this may be due, in part, to the omission of a deposition catalyst. (Kaas et al.1971) The presence of a Si2p spectrum and the subdued presence of the C1s carboxylic acid component indicate that only some anhydride was deposited, as previously found, (Stanicki et al. 2014) again as a monolayer or less. The unexpected presence of the various N1s components indicates contamination, probably by the HNO_3 used in the sample preparation. The peak attributions are found in Table 1.

In an effort to understand the presence of impurities on the surface, particularly as to which can affect the functionalization of the nanoparticles as prodrugs, and whether they can be removed by washing, we carried out a study of the surfaces of the nanoparticles from the second batch, subsequent to dialysis (Mireles et al., submitted). As seen in Table 1 of the

accompanying Data in Brief, while some contaminants can, indeed, be removed by washing, the washing process introduces others.

3.4 FTIR Spectroscopy

Fig. 7 shows the IR spectra of the three SPIONs. The bands and their attributions are found in Table 2, and corroborate the species found by XPS. The presence of oxidized N is attributed to the trace of HNO_3, as well as to oxidized amine (positive SPIONs). The presence of silica demonstrates the attachment of silane chains to the surface (positive and negative), only a monolayer or less, as already noted. In confirmation, the sizes of all the types of SPIONs are, within experimental error, identical.

3.5 TOF-SIMS

TOF-SIMS spectra of the SPIONs, in Fig. 8, confirm the presence of amine groups in positive SPIONs. Na^+ appears in positive spectra, with elevated peak intensity, because Na^+ has a very large ion yield but a low XPS sensitivity, where it is far more difficult to see. While the C1s spectrum of the negative SPIONs was anticipated to be rich in carboxylic acid groups, the intensity found was very low, again supporting the XPS results.

Although it is important to note that TOF-SIMS is not quantitative, a comparison of the high resolution amine peaks in positive SIMS (Fig. 9a) and the carboxylic acid peaks in negative SIMs (Fig. 9b) show that all three types of SPIONs contain both amine and carboxylic acid groups. While the positive SPIONs have the most intense amine peak, both positive and bare SPIONs have more intense carboxylic acid peaks than the negative SPIONs. A summary of the principal peaks is found in Table 3.

4. Discussion

Surface analysis plays an extremely important research role as a fundamental technique in characterizing functionalized SPIONs proposed as drug delivery vehicles. This is because low resolution techniques (e.g., FTIR), cannot satisfactorily confirm that functionalization has occurred, as opposed to the high resolution techniques used in the present paper.

As mentioned earlier, our goal is the characterization of the surface functionalization of SPIONs produced by alkaline coprecipitation, and its reproducibility. In contrast, results found in the literature often lack surface analytical characterizations that confirm the attachment of drugs onto ostensibly functionalized nanoparticles. Further, a lack of reproducibility in nanomaterial fabrication creates a worrisome situation for the research community, as well as for companies that produce and develop products and processes, destined for use in the human body, that use them. One crux of the problem is surely a lack of standards and techniques for surface characterization, and their use in quantifying reproducibility.

Surface Characterization

Our SPIONs showed relatively uniform sizes around 10 nm (Figs. 1 and 2), and spherical shapes (Fig. 1). The increases in average sizes of our positive and negative SPIONs, compared to our bare SPIONs, are around 0.5 and 0.7 nm, respectively (Fig. 6). These results are comparable with hydrodynamic diameters of 9.3 ± 1.4 nm for bare SPIONs, 10.1 ± 1.3 nm for positive SPIONs and 10.4 ± 1.6 nm for negative SPIONs, previously published by us (Mbeh DA et al. 2015); both techniques confirm the essentially identical sizes of our SPIONs, and their small size differences; since both of the silanes used have lengths of > 1 nm, this implies possible silane fragmentation [11] on deposition, and/or only partial functionalization, too low for self-assembly.

The XRD patterns of our SPIONs (Fig. 1) indicate magnetite cores. Their magnetic properties (Fig. 3) indicate reasonably high magnetization (around 26 emu/g), and the absence of a hysteresis loop confirms them to be SPIONs.

The presence of $-NH_2$ and -COOH were confirmed by our XPS (Table 1), FTIR (Table 2) and TOF-SIMS (Table 3) results. These three techniques also showed traces of residual contaminants, as well as cross-contamination; since precautions were taken to avoid cross-contamination, its presence appears to be unavoidable and can affect the chemical surface analysis, as seen in the XPS attributions in Tables 1 and in the accompanying Data in Brief (Mireles et. al., submitted). Examples of contamination abound, such as both positive and bare SPIONs containing amine groups, and negative SPIONs being the least rich in carboxylic acid groups.

Our previous studies (França et al. 2013) on SPIONs manufactured by the thermal decomposition of $Fe(CO)_5$ showed the same characteristics found in the present case: batch-to-batch differences in Tables 1 and 2, and in the accompanying Data in Brief (Mireles et.al., "submitted), hydrocarbon-contaminated surfaces, the absence of a silane layer (although a silane layer may be deposited over a silica layer from the alkaline decomposition of TEOS), amine oxidation and silane fragmentation. The absence of a substantial silane layer deposited onto the bare SPIONs has been found by others using other fabrication schemes, (França et al. 2013, Agnihotri et al. 2013, Boon et al. 2014) making it improbable that this is due to our manufacturing process. Zeta potential measurements, for the SPIONs considered here, were determined previously (Mbeh DA et al. 2015) in water, PBS and culture media containing fetal bovine serum; they were found to have potentials of -25 mV for bare SPIONs, +35 mV for positive SPIONs and -40 mV for negative SPIONs. The negative potential of the bare SPIONs supports our contention of unavoidable contamination during synthesis, and such contamination can be persistent even after dialysis (Mireles et.al., submitted), as our results demonstrate.

5. Conclusions

The surfaces of our SPIONs are only weakly functionalized by direct reaction with silanes, probably due to the catalytic effect of the magnetite core. Further, their manufacture appears to involve unavoidable contamination that can cause problems impacting biomedical applications. In this context, the determination of the presence of contaminants produced by the various manufacturing processes, and the extent of reproducibility are important in monitoring SPION purity and eventual use as prodrugs for use in the human body. Finally, based on the unavoidable presence of unexpected chemical groups, it may well be that bare SPIONs, when PEGylated with functionalized PEGs, offer the best opportunity as prodrugs because of the ability to control reproducibility.

6. Acknowledgements

We thank the Fonds de recherche du Québec (FQRNT) and the Groupe de recherche en sciences et technologies biomédicales (GRSTB) for support. We thank Josianne Lefebvre for assistance in processing the XPS and TOF-SIMs data, and Rafaella Oliveira do Nascimento, for contributions during discussions.

The ARC (research contract AUWB-2010—10/15-UMONS-5), the FNRS, the Walloon Region, the COST TD1004 and TD1402, the UIAP VII program and the Center for Microscopy and Molecular Imaging (CMMI, supported by the European Regional Development Fund and the Walloon Region) are thanked for their support.

References

Afkhami F, Taherkhani S, Mohammadi M, Martel S. Encapsulation of magnetotactic bacteria for targeted and controlled delivery of anticancer agents for tumor therapy. Conf Proc IEEE Eng Med Biol Soc 2011; 6668 - 6671.

Agnihotri S, Mukherji S, Mukherji S. Immobilized Silver Nanoparticles Enhance Contact Killing and Show Highest Efficacy: Elucidation of the Mechanism of Bactericidal Action of Silver. Nanoscale 2013; 5: 7328-7340.

Boon MS, Mariatti M. Silane treatment of magnetite filler and its effect on the properties of magnetite-filled epoxy thin-film composites. Polym. Bull 2014; 71: 3333–3346.

Bridot JL, Stanicki D, Laurent S, Boutry S, Gossuin Y, Leclère P, Lazzaroni R, Vander-Elst L, Muller RN. New carboxysilane-coated iron oxide nanoparticles for nonspecific cell labelling. Contrast Media Mol. Imaging 2013; 8: 466–474.

Brosseau C, Youssef JB, Talbot P, Konn AM. Electromagnetic and Magnetic Properties of Multicomponent Metal Oxides Heterostructures: Nanometer Versus Micrometer-Sized Particles. J. Appl. Phys 2003; 93(11): 9243–9256.

Davydov V, Rakhmanina A, Kireev I, Alieva I, Zhironkina O, et al. Solid state synthesis of carbon-encapsulated iron carbide nanoparticles and their interaction with living cells. J. Mater. Chem. B 2014; 2: 4250-4261.

Dickinson GM, Bisno AL. Infections associated with indwelling devices: concepts of pathogenesis; infections associated with intravascular devices. Antimicrob Agents Chemother 1989; 33(5): 597–601.

Felfoul O, Mokrani N, Mohammadi M, Martel S. Effect of the Chain of Magnetosomes Embedded in Magnetotactic Bacteria and their Motility on Magnetic Resonance Imaging. Conf Proc IEEE Eng Med Biol Soc 2010; 4367-4370.

Forge D, Roch A, Laurent S, Tellez H, Gossuin Y, Renaux F, Vander-Elst L, Muller RN. Optimization of the Synthesis of Superparamagnetic Contrast Agents by the Design of Experiments Method. J. Phys. Chem. C 2008; 112, 19178–19185.

França R, Zhang XF, Veres T, Yahia L'H, Sacher E. Core-shell nanoparticles as prodrugs: possible cytotoxicological and biomedical impacts of batch-to-batch inconsistencies. J Colloid Interface Sci. 2013; 1; 389(1): 292-7.

Frankel RB, Bazylinski DA, Johnson MS, Taylor BL. Magneto-Aerotaxis in Marine Coccoid Bacteria. J Biophysical Journal 1997; 73: 994-1000.

Gupta AK, Wells S. Surface-modified superparamagnetic nanoparticles for drug delivery: preparation, characterization, and cytotoxicity studies. IEEE transactions on nanobioscience 2004; 3(1): 66-73.

Kaas R, Kardos JL. The Interaction of Alkoxysilane Coupling Agents with Silica Surfaces. Polym Eng. Sci, 1971; 11: 11–18.

Li YF, Chen C. Fate and toxicity of metallic and metal-containing nanoparticles for biomedical applications. Small, 2011; 7: 2965–2980.

Liu R-t, Liu J, Tong J-q, Tang T. Kong WC, Wanga X-w, Lib Y, Tang J-t. Heating effect and biocompatibility of bacterial magnetosomes as potential materials used in magnetic fluid hyperthermia. Progress in Natural Science: Materials International 2012; 22(1): 31–39.

Mbeh DA, França R, Merhi Y, Zhang XF, Veres T, Sacher E, Yahia, L'H. In vitro biocompatibility assessment of functionalized magnetite nanoparticles: biological and cytotoxicological effects. J Biomed Mater Res A 2012; 100(6): 1637-46

Mbeh DA, Mireles LK, Stanick D, Tabet L, Maghni K, Laurent S, Sacher E and Yahia L'H. Human Alveolar Epithelial Cell Responses to Core−Shell Superparamagnetic Iron Oxide Nanoparticles (SPIONs). Langmuir 2015; 31: 3829−3839.

Mireles LK, Sacher E, Yahia L´H, Laurent S and Stanicki D. Washing effect on superparamagnetic iron oxide nanoparticles. International Journal of Biochemistry & Cell Biology, "submitted"

Nablo BJ, Prichard HL, Butler RD, Klitzman B, Schoenfisch MH. Inhibition of implant associated infections via nitric oxide release. Biomaterials 2005; 26(34): 6984-6990.

Pham D-D, Fattal E and Tsapis N. Pulmonary drug delivery systems for tuberculosis treatment. Internat. J. Pharmaceutics 2015; 478: 517–529.

Poulin S, Franca R, Moreau-Bélanger L, Sacher E. Confirmation of X-ray Photoelectron Spectroscopy Peak Attributions of Nanoparticulate Iron Oxides, Using Symmetric Peak Component Line Shapes. J. Phys. Chem. C 2010; 114 (24): 10711–10718.

Rao S, Tan A, Thomas N and Prestidge CA. Perspective and potential of oral lipid-based delivery to optimize pharmacological therapies against cardiovascular diseases. J. Controlled Release 2014; 193: 174–187.

Sawant RM, Sawant RR, Gultepe E, Nagesha D, Papahadjopoulos-Sternberg N, Sridhar S, Torchilin VP. Nanosized cancer cell-targeted polymeric immunomicelles loaded with superparamagnetic iron oxide nanoparticles. J. Nanopart. Res 2009; 11: 1777–1785.

Stanicki D, Boutry S, Laurent S, Wacheul L, Nicolas E, Crombez D, Vander Elst L, Lafontaine DLJ, Muller RN. Carboxy-silane coated iron oxide nanoparticles: a convenient platform for cellular and small animal imaging. J. Mater. Chem. B 2014; 2: 387-397

Tassa C, Shaw SY, Weissleder R. Dextran-coated iron oxide nanoparticles: a versatile platform for targeted molecular imaging, molecular diagnostics, and therapy. Acc. Chem. Res 2011; 44(10): 842-52.

Trampuz A, Widmerm AF. Infections associated with orthopedic implants. Clin. Infect. Dis 2001; 2(33): S94 – S106.

Wilcox M, Kite P, Mills K, Sugden S. In situ measurement of linezolid and vancomycin concentrations in intravascular catheter-associated biofilm. J Antimicrob Chemother 2001; 47: 171–175.

Yamanaka M, Hara K, Kudo J. Bactericidal Actions of a Silver Ion Solution on Escherichia coli, Studied by Energy-Filtering Transmission Electron Microscopy and Proteomic Analysis. Appl Environ Microbiol 2005; 71(11): 7589–7593.

Zhang X, Mansouri S, Mbeh DA, Yahia L'H, Sacher E, Veres T. Nitric Oxide Delivery by Core/shell Superparamagnetic Nanoparticle Vehicles with Enhanced Biocompatibility. Langmuir 2012; 28 (35): 12879–12885.

Healthcare-associated Infections: A backgrounder. Online. January 2009. Available from: http://cupe.ca/updir/healthcare-associated-infections-cupe-backgrounder.pdf

Graphical Abstract

Comparison, reproducibility and washing effect of silane-functionalized iron oxide nanoparticles

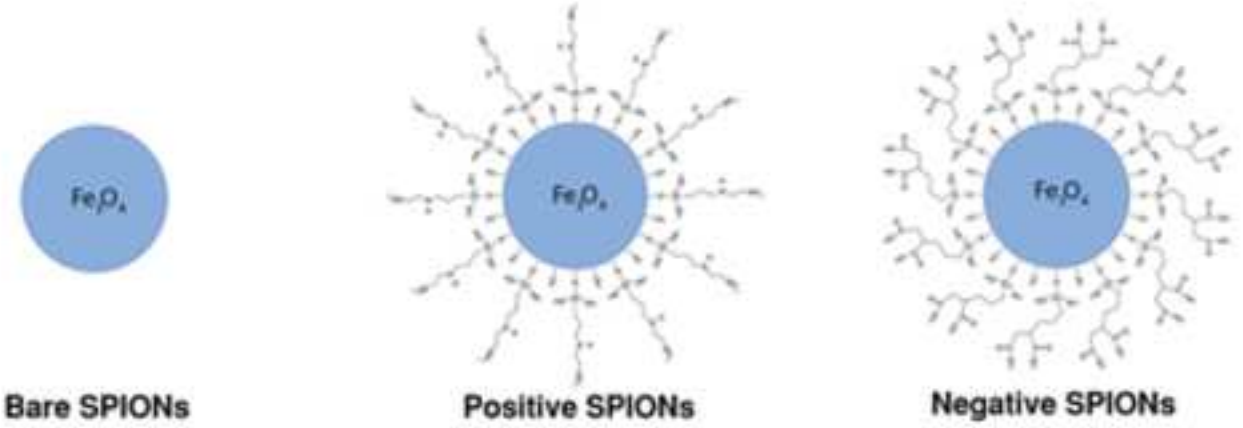

Highlights

- Detailed surface characterizations of core-shell superparamagnetic magnetite nanoparticles to probe the chemistry of the surface, predict future functionalization for drug delivery, and understand batch-to-batch repeatability, protein corona formation and cytotoxicity effects
- Comparison of product reproducibility and washing effect by dialysis on surfaces
- Batch-to-batch variation of surface chemistryis found in all the samples

Figure(s)

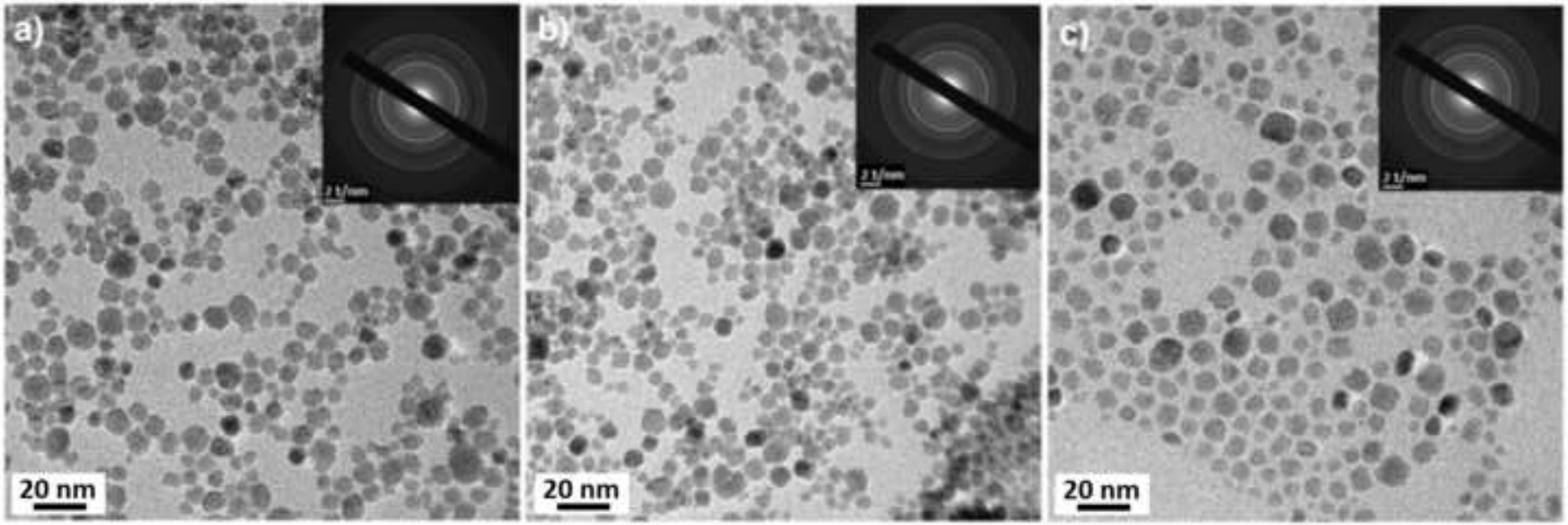

Figure(s)

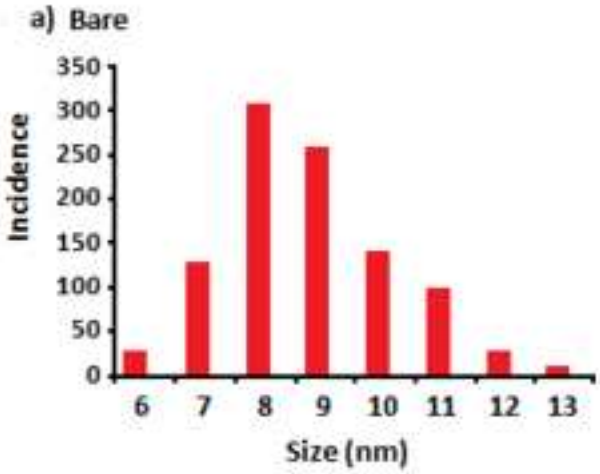

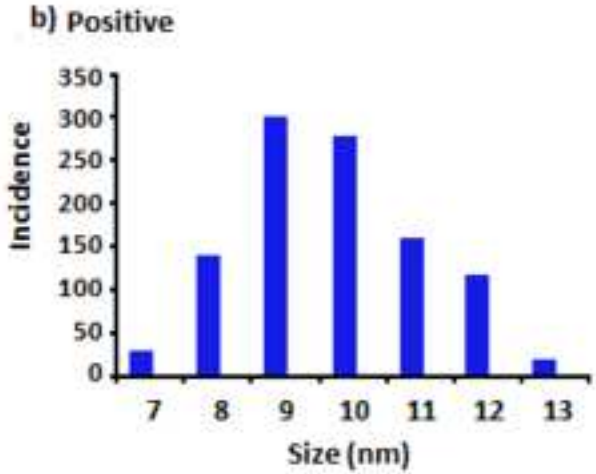

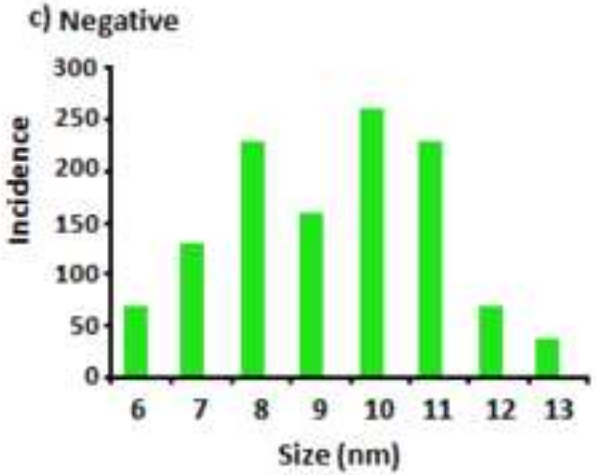

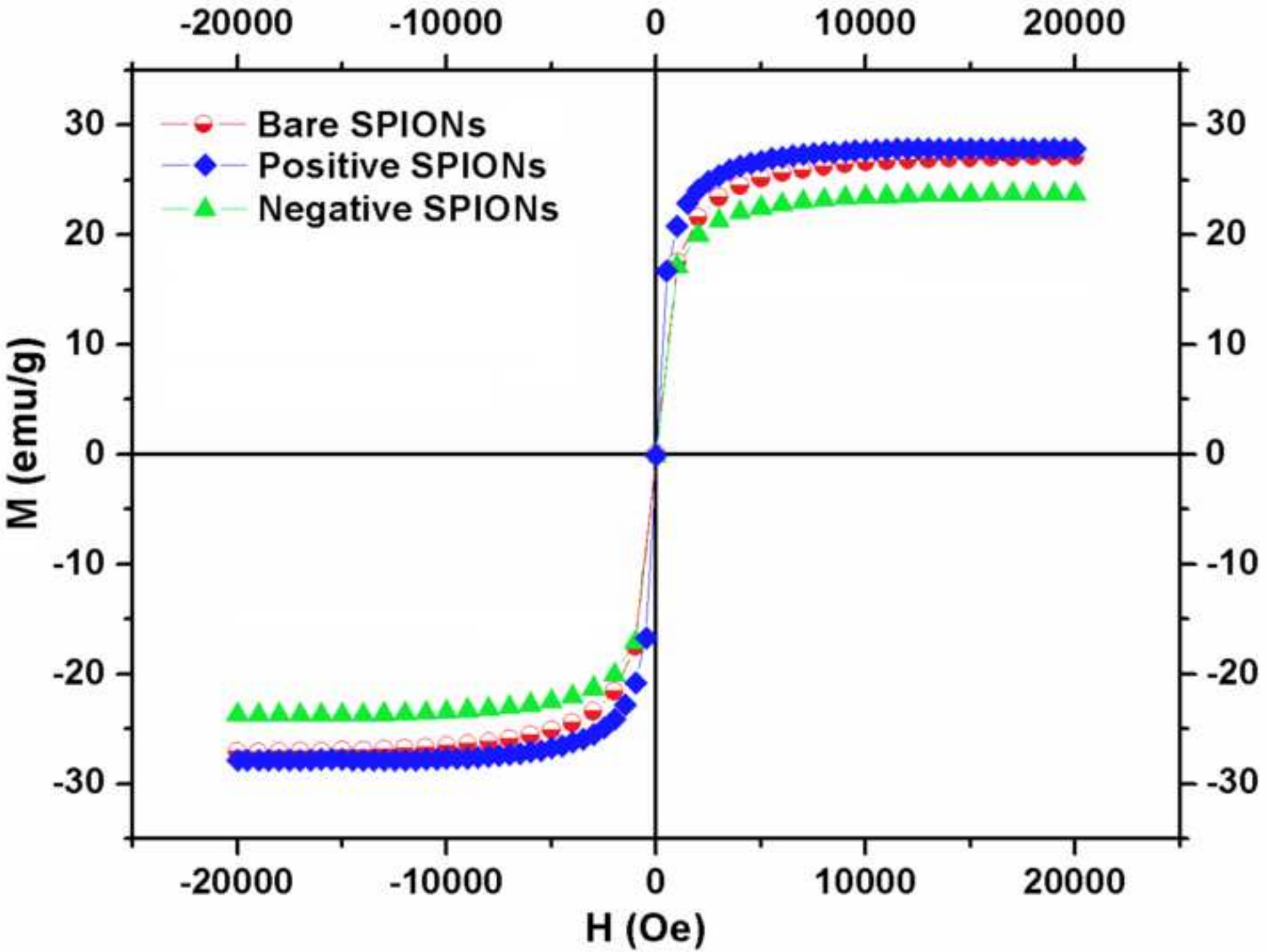
-20000
-10000
0
10000
20000
30
20
10
0
-10
-20
-30
Bare SPIONs
Positive SPIONs
Negative SPIONs
M (emu/g)
H (Oe)

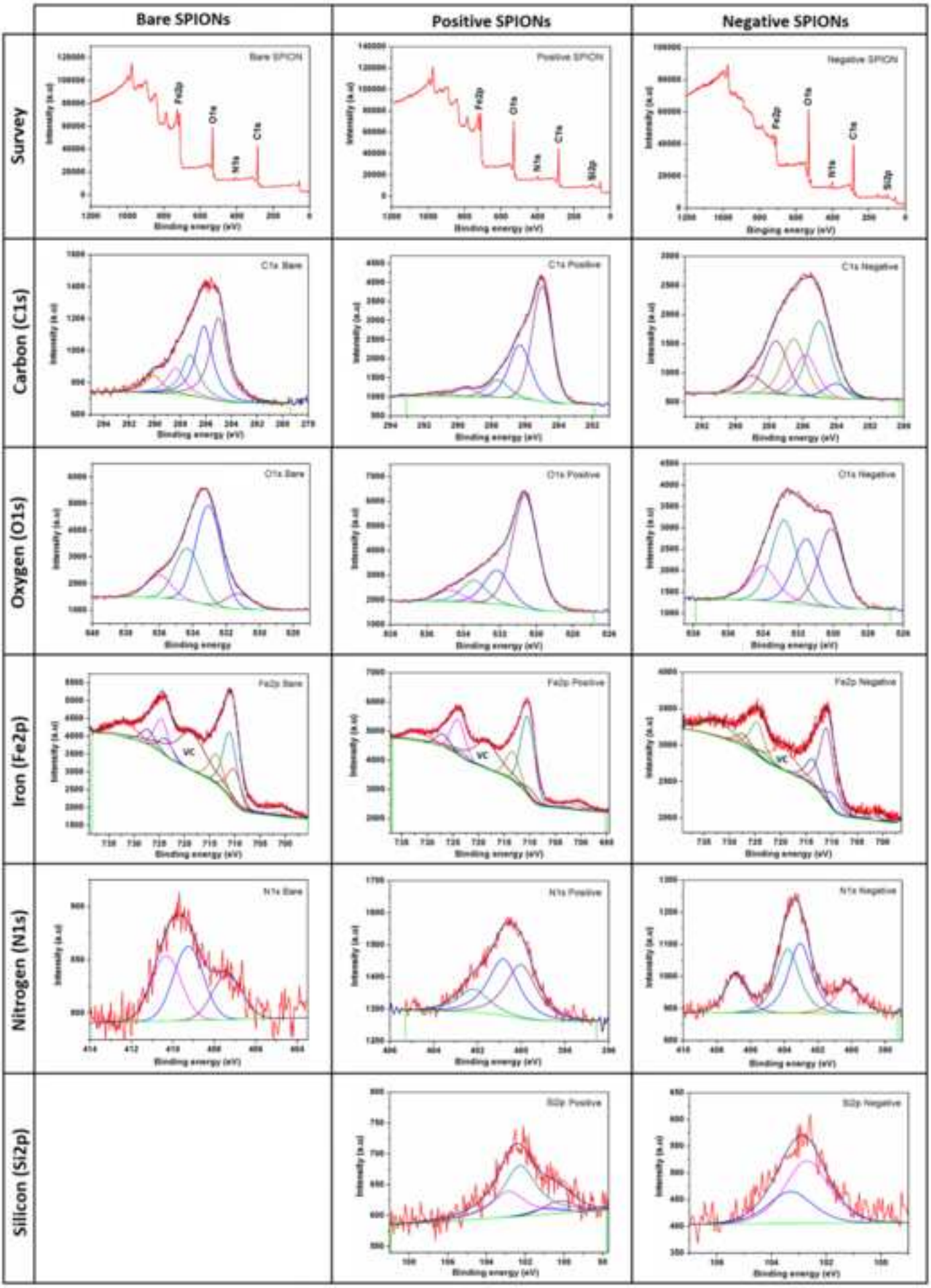

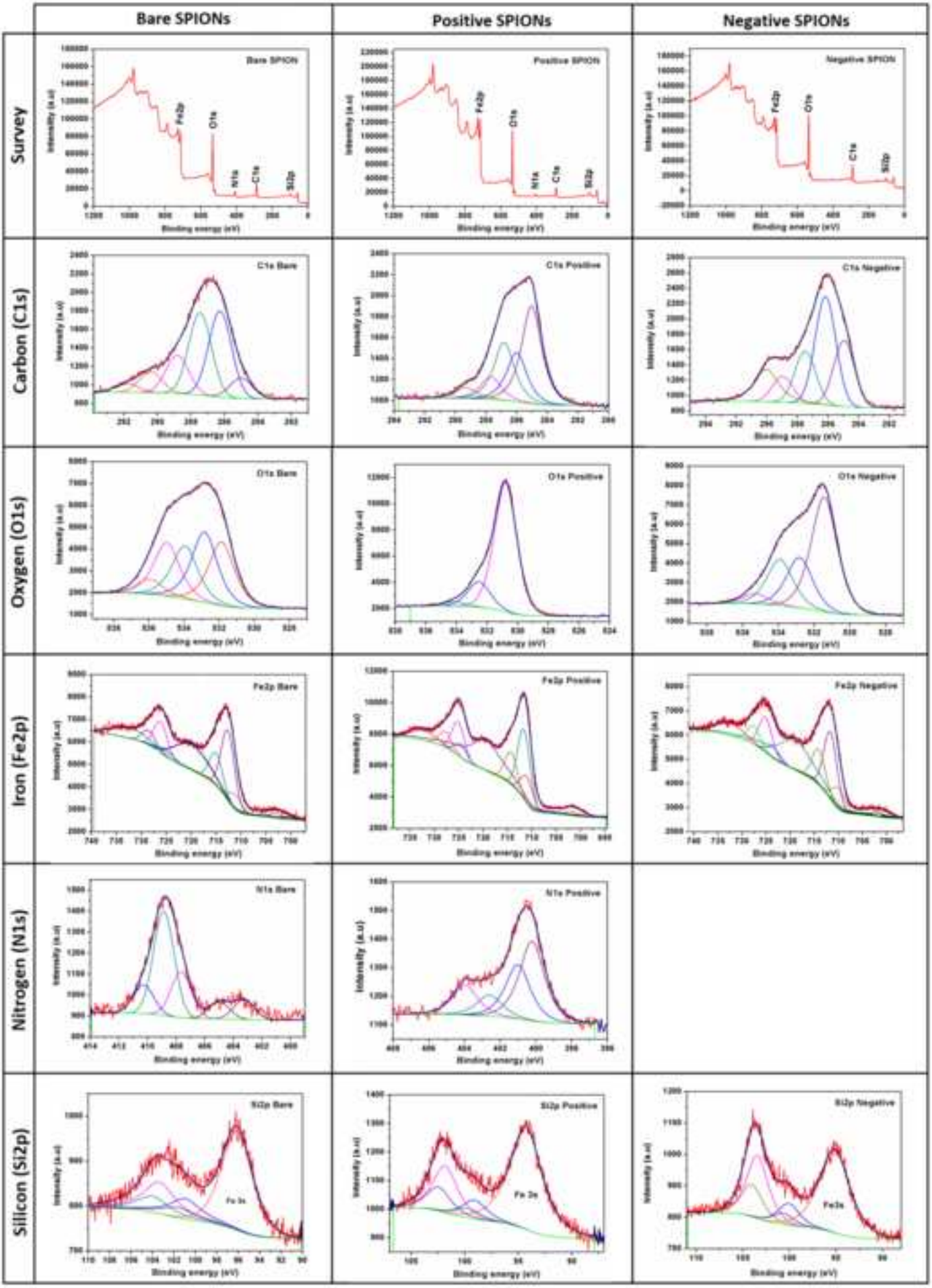

Figure(s)

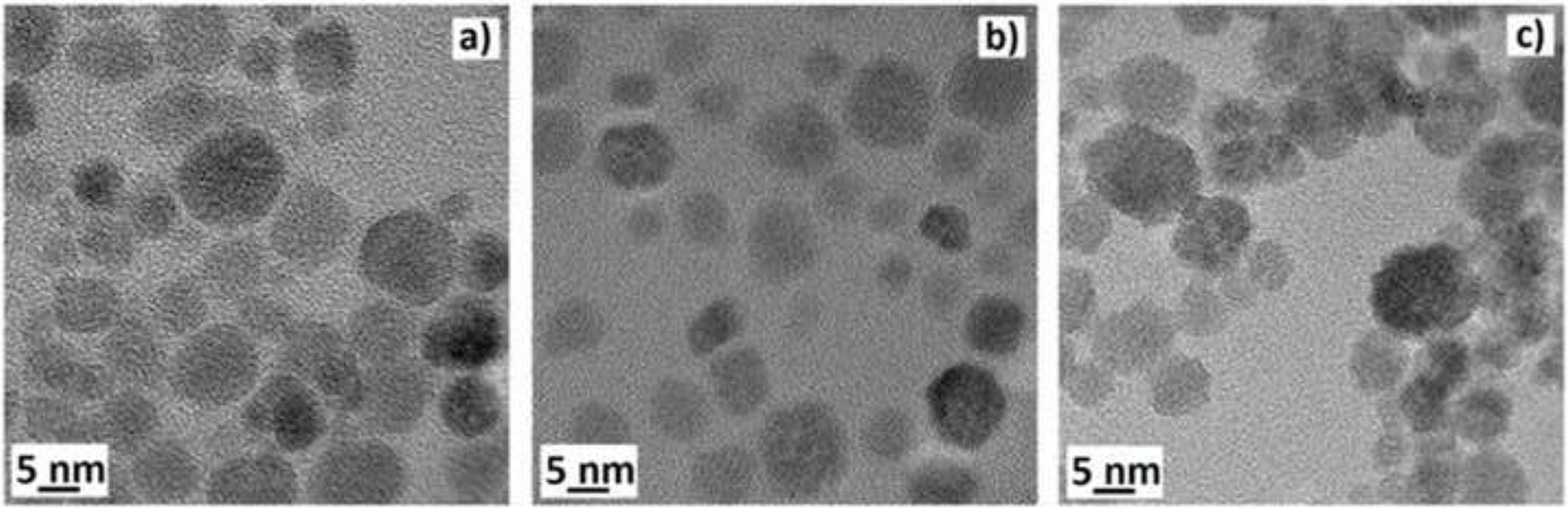

Figure(s)

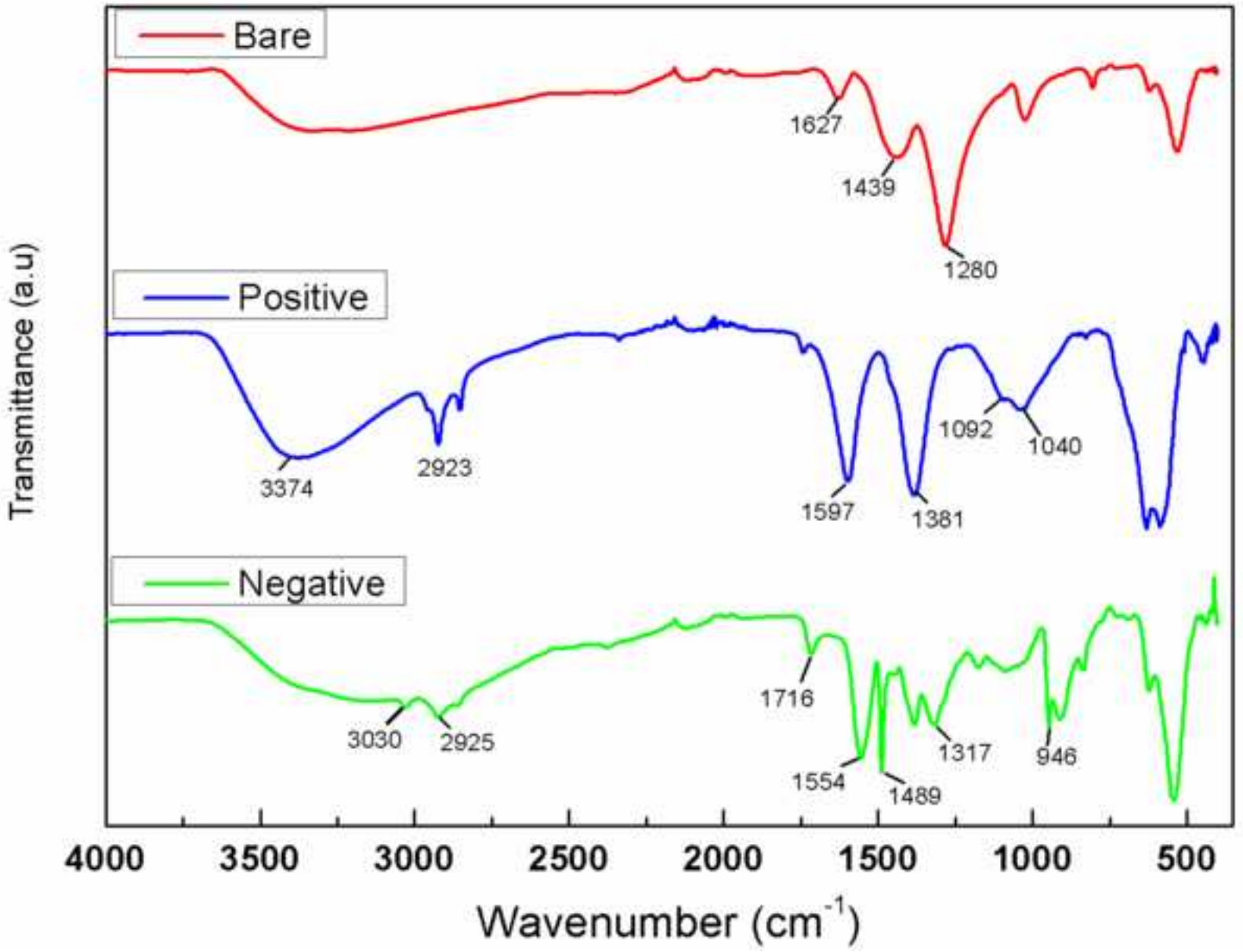
Bare
1627
1439
1280
Positive
3374
2923
1597
1381
1092
1040
Negative
3030
2925
1716
1554
1489
1317
946
Transmittance (a.u)
4000
3500
3000
2500
2000
1500
1000
500
Wavenumber (cm-1)

Figure(s)

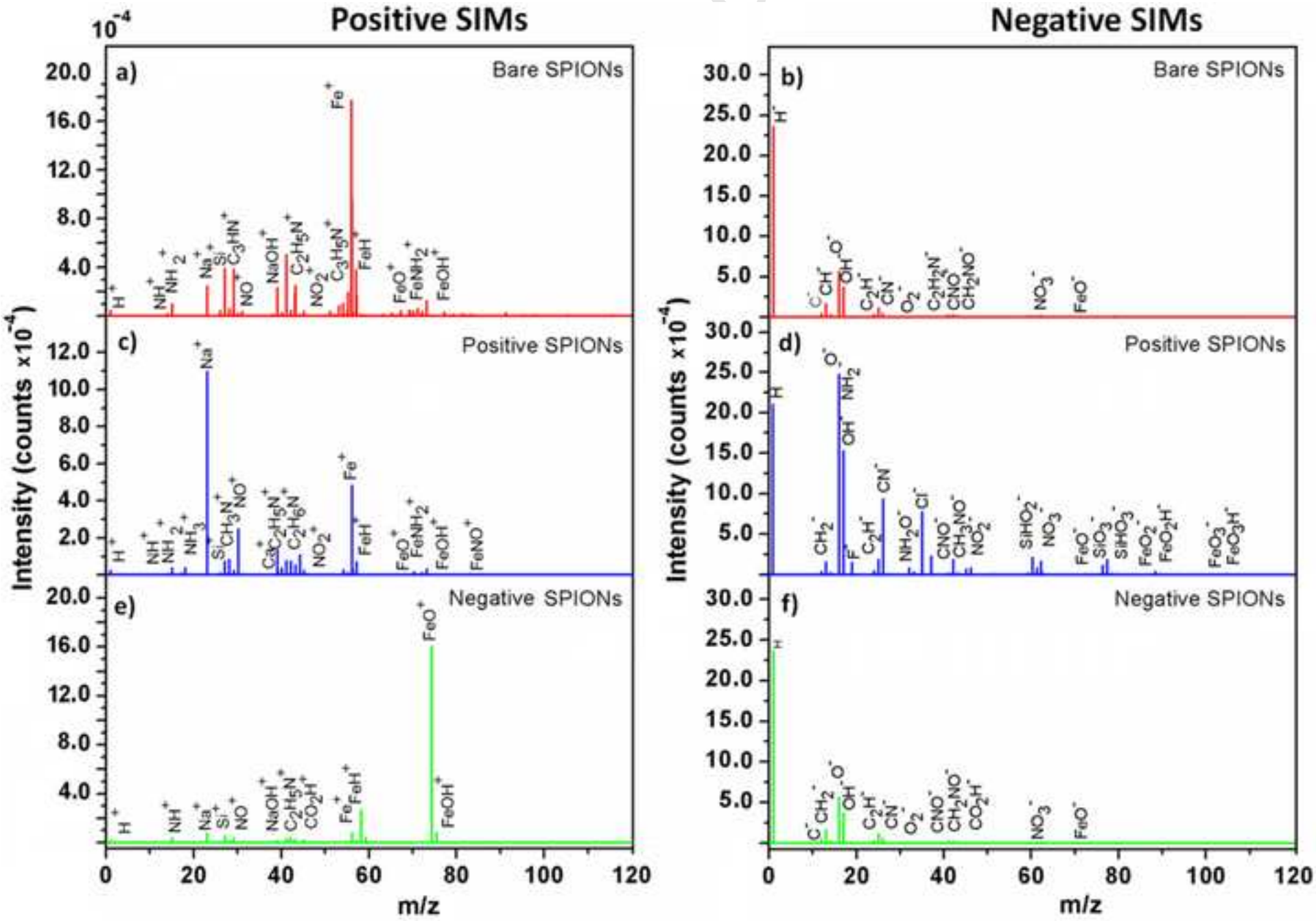
Positive SIMs
Negative SIMs
a)
Bare SPIONs
b)
Bare SPIONs
c)
Positive SPIONs
d)
Positive SPIONs
e)
Negative SPIONs
f)
Negative SPIONs
Intensity (counts x10^-4)
m/z

Figure(s)

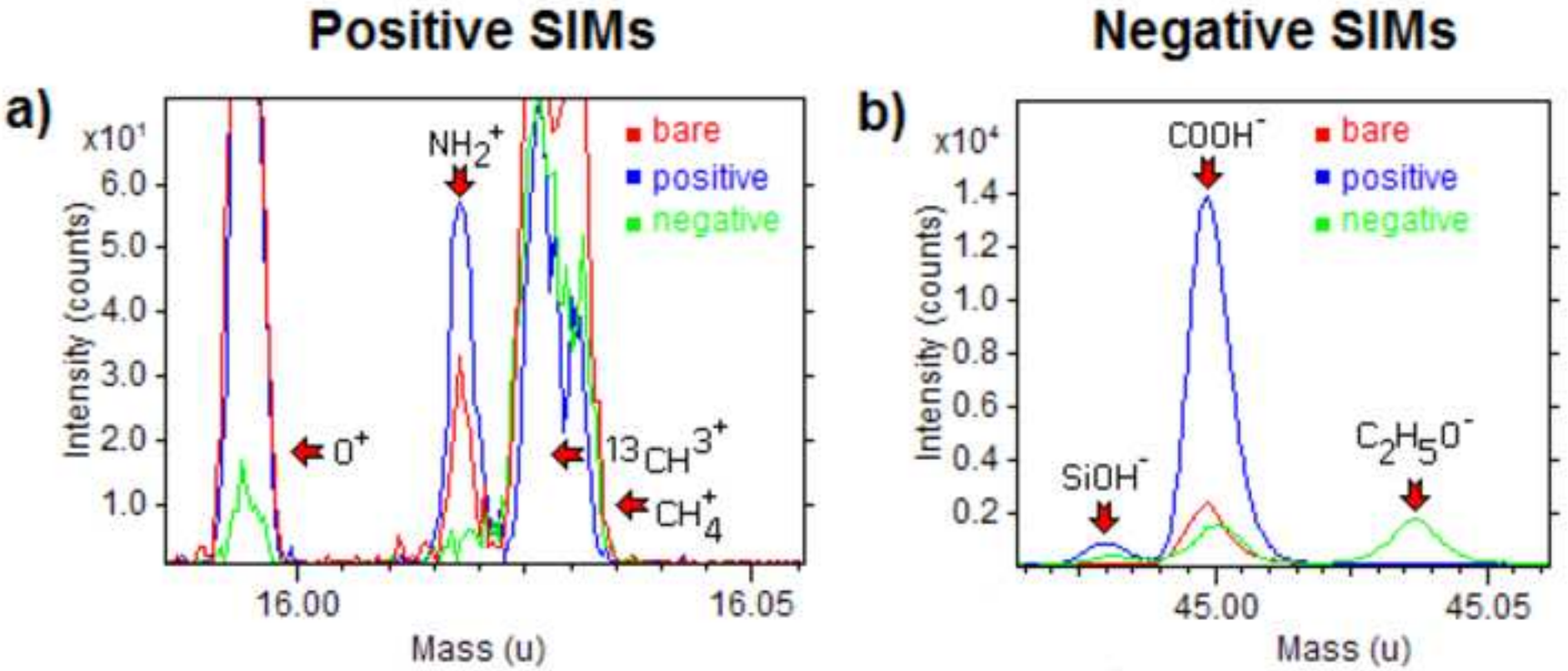
Positive SIMs
a)
x10¹
6.0
5.0
4.0
3.0
2.0
1.0
Intensity (counts)
NH2+
O+
13CH3+
CH4+
bare
positive
negative
16.00
16.05
Mass (u)
Negative SIMs
b)
x10⁴
1.4
1.2
1.0
0.8
0.6
0.4
0.2
Intensity (counts)
COOH-
SiOH-
C2H5O-
bare
positive
negative
45.00
45.05
Mass (u)

Captions for Illustrations and Tables

Fig. 1 TEM images of: a) bare, b) positive and c) negative SPIONs.

Fig. 2 Size distributions of: a) bare, b) positive and c) negative SPIONs.

Fig. 3 Magnetization curves of SPIONs

Fig. 4 High resolution XPS spectra of bare, positive and negative SPIONs (first batch).

Fig. 5 High resolution XPS spectra of positive, negative and bare SPIONs (second batch).

Fig. 6 HRTEM photomicrographs of a) positive, b) negative and c) bare SPIONs. Each sample lacks a visible surface coating.

Fig. 7 IR spectra of bare, positive and negative SPIONs.

Fig. 8 Positive and negative SIMS spectra of (a, b) bare, (c, d) positive and (e, f) negative SPIONs.

Fig. 9 High resolution SIMS comparisons of a) NH_2 peaks (M: 16.01), b) COOH peaks (M: 44.99), of the SPIONs.

Table 1 Summary of XPS deconvolutions of SPIONs from the first and second batches.

Table 2 Attribution of FTIR peaks from the first batch.

Table 3 Masses and attributions of the fragments found in SPIONs from the first batch.

Tables

Table 1 Summary of XPS deconvolution of SPIONs from the first and second batches.

COMPARISON FIRST AND SECOND BATCHES - Peak Positions						
Suggested Attribution	**Bare SPIONs (eV)**		**Positive SPIONs (eV)**		**Negative SPIONs (eV)**	
	First batch	**Second batch**	**First batch**	**Second batch**	**First batch**	**Second batch**
C-Si			284.1 (~0)		284.1	
C-C	285.0	285.0	285.0	285.0	285.0	285.0
C-N			285.8	286.0	285.8	
C-O	286.1	286.3	286.1	286.8	286.5	286.2
C=O	287.2	287.5	287.5	287.7	287.6	287.5
COOH	288.4 (***)	288.8	289.5	289.4	289.2	288.9
COO-	290.1	290.4				290.0
***		291.8				
Fe-O	531.0		530.6	530.8 + Fe-OH	530.1	
Fe-OH					531.5 + O-Si	
C=O	532.9 + Fe-OH	531.8 + Fe-OH	532.2 + O-Si	532.5	532.8	531.4 + Fe-OH
C-O	534.1 + C-OH	532.8	533.4		533.9 + C-OH	532.8
C-OH/ O-N			534.7	534.1		533.9
***	536.8	535.0				535.3
***		536.0				
NH_2			400.1	400.2	400.2	
NH_3^+			400.8	401.0		
NO			402.2	402.6		
***						
NO_2		403.3			403.0	
***		405.0		404.0	403.8	
NO_3 organic	407.2	407.7			406.8	
NO_3 inorganic	408.3	408.8				
***	409.5	410.3				
Fe II octa	710.1	711.1	709.7	711.0	709.7	710.0
Fe III octa	711.0	712.6	710.4	711.8	711.0	711.6
Fe III tetra	713.7	715.0	713.4	714.2	713.7	714.1
Si-C				99.2		100.1
Si-O		101.0	100.2 + Si-C			
$Si-O_2$			102.3	101.9		
$Si-O_3$		103.4			102.7	103.4

Table 2 Attribution of FTIR peaks from the first batch.

Sample	Wavelength (cm^{-1})	Attribution
Bare	1627	R-O-NO_2
	1280	NO_3^-
Positive	3374	NH_n
	1741	C=O
	1597	RNH_2, R_2NH
	1381	R_2NH, RNO_2, NO_3^-
	1092	Si-O-Si
	1040	Si-O-C
Negative	3030	OH
	2925	C−H
	1716	C=O
	1554	COO^-
	1489	COO^-
	1374	RNO_2, NO_3^-
	1317	C−O
	1175	Si−O−Si
	1090	Si-O-C
	946	OH
	911	OH

Table 3 Masses and attributions of the fragments found in SPIONs from the first batch.

Species	Mass (D)	Species	Mass (D)
C	12.00	CO_2H	44.99
NH	15.02	NO_2	45.99
O	15.99	Fe	55.93
NH_2	16.01	FeH	56.94
OH	17.00	FeO	71.92
NH_3	17.02	FeOH	72.93
Na	22.98	FeNO	85.93
NO	29.99	FeO_2	87.92